Arabian Journal of Chemistry (2023) **16**, 104497

King Saud University

Arabian Journal of Chemistry

www.ksu.edu.sa
www.sciencedirect.com

ORIGINAL ARTICLE

Ameliorating the sensitivities, thermal and combustion properties of RDX by *in situ* self-assembly TA-Pb/Cu shells to RDX surface

Guanchao Lan [a,b], Guangyuan Zhang [b], Jinjie Shen [b], Guoliang Jin [b], Jianlong Wang [a], Jing Li [c,*]

[a] *School of Chemical Engineering and Technology, North University of China, Taiyuan 030051, China*
[b] *Gansu Yin Guang Chemical Industry Group Co. Ltd., Baiyin 730900, China*
[c] *School of Materials Science and Engineering, North University of China, Taiyuan 030051, China*

Received 12 September 2022; accepted 18 November 2022
Available online 9 December 2022

KEYWORDS

RDX@TA-Pb/Cu;
In situ self-assembly coating;
Catalytic

Abstract In order to ameliorate the sensitivities, thermal and combustion properties of cyclotrimethylenetrinitramine (RDX), tannic acid (TA) is used to react with lead and copper via *in situ* self-assembly to coat RDX for preparing RDX@TA-Pb/Cu microcapsules. The structures of RDX@TA-Pb/Cu microcapsules are characterized by X-ray photoelectron spectroscopy (XPS), X-ray diffraction (XRD) and Fourier-transform infrared spectra (FT-IR). The surface topography of RDX@TA-Pb/Cu microcapsules are characterized by scanning electron microscope (SEM) and energy dispersive spectroscopy (EDS). The mechanical sensitivities and explosion points of RDX@TA-Pb/Cu microcapsules are measured to study the influence of TA-Pb/Cu shells on mechanical and thermal safeties of RDX. The non-isothermal properties of RDX@TA-Pb/Cu microcapsules are characterized by differential scanning calorimetry (DSC). The catalytic effects of TA-Pb/Cu shells on RDX are characterized by accelerating rate calorimeter (ARC). The residues of RDX@TA-Pb/Cu microcapsules after combustion in air are collected and characterized by SEM and XRD to further study the catalytic effect of TA-Pb/Cu shells. The study results show that a 150 nm TA-Pb/Cu shells are uniformly coated on RDX surfaces. The chemical structure of RDX maintains constant during *in situ* self-assembly coating process. The mechanical and thermal safeties of RDX are enhanced after coating with TA-Pb/Cu shells. The decomposition and combustion property of RDX can be catalyzed by TA-Pb/Cu, and the catalytic effects of *in situ* self-assembly coating are better than that of physical mixing. The RDX@TA-Pb/Cu microcapsules

* Corresponding author.
E-mail address: 20210064@nuc.edu.cn (J. Li).
Peer review under responsibility of King Saud University.

Production and hosting by Elsevier

https://doi.org/10.1016/j.arabjc.2022.104497

can be used in RDX based composite modified double base (CMDB) propellants.

1. Introduction

High energy explosives are important components of composite modified double base (CMDB) propellants (Elbasuney et al., 2017; Liu et al., 2018; Damse et al., 2007), in that high energy explosives can release energy rapidly and produce a large amount of gas with high temperature when burning. The addition of high energy explosives can endow CMDB propellants high energy level and controllable signature (Stepanov et al., 2013; Zhang et al., 2022). Therefore, CMDB propellants containing high energy explosives have wide useage in missile and rocket engine as power source (Dubey et al., 2012; Ou, 2014). Cyclotrimethylenetrinitramine (RDX, Fig. 1a) is one of the most commonly used high energy explosives to prepare CMDB propellants, because of the low press and excellent energetic characteristics (Liu et al., 2001). However, high pressure exponent and low burning rate are two main shortcomings of RDX-CMDB propellants. Former studies show that organic lead copper composites salts are effective combustion catalyst that can adjust the pressure exponent and improve the burning rate of RDX-CMDB propellants (Jiang et al., 2020; He et al., 2021). There are two kinds of catalytic element (lead and copper) in catalyst molecule, resulting in a complementary to strong synergistic effect, and thus improve the catalytic effect. Therefore, the addition of organic lead copper composites salts is important for ameliorating the combustion properties of RDX-CMDB propellants.

In traditional RDX-CMDB propellants, the organic lead copper composites salts catalysts are usually added by physical mixing that may result in non-uniform mixing. Moreover, in traditional RDX-CMDB propellants, RDX and organic lead copper composites salts catalysts are separated by adhesive, *i.e.* RDX crystals are not contact with catalysts directly. Therefore, the catalytic effect of organic lead copper composites salts catalysts can not be sufficiently exploited in traditional RDX-CMDB propellants. It is an effective strategy to enhance the catalytic effect of catalysts by *in situ* or *ex situ* method to prepare core@shell structures (He et al., 2022). Due to the unique ability of forming unifirm film and controllable film thickness, atomic layer deposition (ALD) is a promising method to achieve the surface modification of energetic materials (Adhikari et al., 2018; Zhang et al., 2017; Yang et al., 2015). Graphene dispersion is a useful strategy to ameliorate the mechanical properties of energetic materials (He et al., 2022), because the quasi layered graphene can slide when suffered external stimuli. Preparing polymer bonded explosives (PBXs) via *ex situ* coating is one of the most commen used techniques for the desensitization of high explosives (Lan et al., 2020), which has been successfully used to desensitize many high sensitive explosives (Lan et al., 2020; Xiao et al., 2021).

In situ self-assembly coating technology can introduce catalysts shells to RDX surface by chemical reaction occurred on RDX surface. The catalytic element (lead and copper) of catalysts shells can compactly and uniformly contact with RDX surface, and thus enhance the catalytic effects. In addition, *in situ* self-assembly coating technique can facilitate extraordinarily high coverage and shell strength owing to the chemical reaction (Lan et al., 2020), which may further enhance thermal stability and decrease mechanical sensitivity of RDX. *In situ* reaction technology has been successfully applied in aluminum powder modification field (Xiao and Liang, 2021; Yang et al., 2022; He et al., 2018; Li et al., 2020), energetic materials amelioration field (Zhang et al., 2019; Gong et al., 2017; Zhao and Zhang, 2011; Lan et al., 2022; Xu and Zhu, 2022) and catalytic field (Zou et al., 2022; Le et al., 2022; Gong et al., 2020; Gong et al., 2021; Guo et al., 2014); *etc*. Therefore, it is an effective method to ameliorate RDX by establishing shell on RDX surface through *in situ* self-assembly coating.

Tannic acid (TA, Fig. 1b), a polyphenolic compound widely found in plants with low price (Wei et al., 2018; Ejima et al., 2013; Yurtsever and Şengil, 2009; Şengil and Özacar, 2008), has abundant phenolic hydroxyl groups that can easily react with Pb^{2+} and Cu^{2+} ions to form polymer-like TA-Pb/Cu metal-phenolic networks by self-assembly (Sánchez-Martín et al., 2011; Lan et al., 2022; Näslund and Persson, 2022). The unreacted phenolic hydroxyl groups of TA-Pb/Cu metal-phenolic networks can form strong non-bonding interaction with itro group of RDX, resulting a good coating effect. The high strength TA-Pb/Cu shells on RDX surfaces like armors that can protect the core RDX when suffering external stimulus, and thus enhance the safety of RDX. The lead and copper of TA-Pb/Cu shells can complementally catalyse the decomposition and combustion of RDX, and thus achieve the goal of ameliorating the pressure exponent and burning rate of RDX-CMDB propellants. The shell thickness of TA-Pb/Cu catalysts can be controlled by *in situ* self-assembly coating times. In addition, compared with pure RDX, the specific surface areas of composites are much higher and thus the adhesive accessible areas are higher, resulting in better mechanical properties.

In this study, RDX@TA-Pb/Cu microcapsules are prepared via *in situ* self-assembly coating process to achieve surface catalytic and enhance safety of RDX. The structure and coating effect are characterized by X-ray photoelectron spectroscopy (XPS), X-ray diffraction (XRD), Fourier-transform infrared spectra (FT-IR) and scanning electron microscope (SEM). The performance of RDX@TA-Pb/Cu microcapsules are compared with physical mixtures of RDX + TA-Pb/Cu through differential scanning calorimetry (DSC) and accelerating rate calorimeter (ARC) to study the catalytic effects of *in situ* self-assembly coating process and physical mixing.

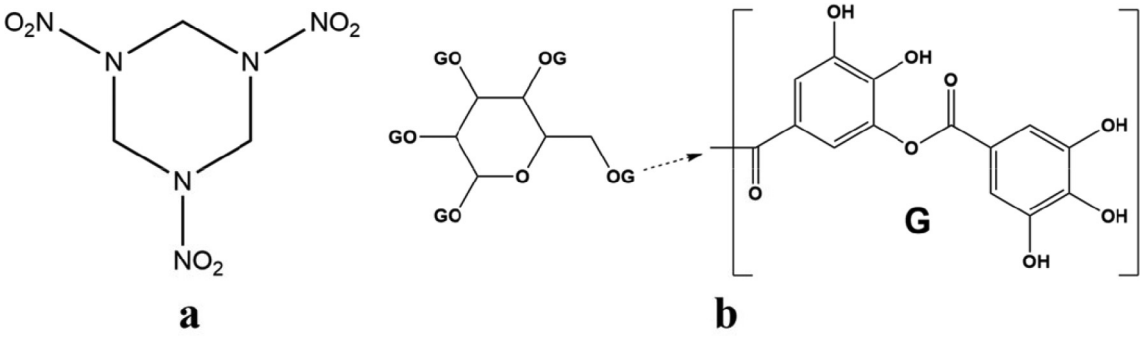

Fig. 1 Molecular structure of RDX (a) and TA (b).

2. Experimental details

2.1. Materials

RDX, provided by Gansu Yin Guang Chemical Industry Group Co. ltd, were purified by recrystallization, and their mass fraction purity was greater than 0.995. TA, Tris-Bis, Pb$(NO_3)_2$ and Cu$(NO_3)_2$ were analytical grade and purchased from a local reagent factory without further purification.

2.2. Preparation of RDX@TA-Pb/Cu microcapsules

At 25 °C, 1.0 g TA and 50 mL deionized water were added into 250 mL three-necks flask and stirred at this temperature until TA is completely dissolved. Then, 10 g RDX particles were added to TA solution and stirred for 30 min to disperse. Then, 180 mg Cu$(NO_3)_2$ and 320 mg Pb$(NO_3)_2$ were added to the above suspension and stirred for 30 min to supply Cu^{2+} and Pb^{2+}. Tris-Bis was then added into the above suspension to adjust the pH value to 7–8. The resulted suspension was stirred at 25 °C for 1 h and then filtered and washed with deionized water. The obtained RDX@TA-Pb/Cu microcapsules were dried in a vacuum oven at 50 °C for 8 h. Repeat above procedures five times to increase the thickness of TA-Pb/Cu shells.

2.3. Characterization of RDX@TA-Pb/Cu microcapsules

The structure of RDX@TA-Pb/Cu microcapsules were characterized by X-ray photoelectron spectroscopy (XPS, Thermo Scientific K-Alpha), X-ray diffraction (XRD, X'Pert PRO MPD Diffractometer) and Fourier-transform infrared spectra (FT-IR, Bruker VERTEX 80), respectively. The surface morphology of RDX@TA-Pb/Cu microcapsules were investigated by scanning electron microscope (SEM, Zeiss Sigma 300) and energy dispersive spectroscopy (EDS). Mechanical sensitivities and explosion points of RDX@TA-Pb/Cu microcapsules were measured using GJB 772A to study the amelioration effects of TA-Pb/Cu shells on mechanical and thermal safety of RDX. Differential scanning calorimetry (DSC, NETZSCH 200 F3) was used to study the non-isothermal decomposition properties of RDX@TA-Pb/Cu microcapsules with a heating rate of 10 $K{\cdot}min^{-1}$. Accelerating rate calorimeter (ARC, NETZSCH ARC 254) was used to study the catalytic effects of TA-Pb/Cu on RDX thermal decomposition. The combustion residues are collected and characterized by SEM and XRD to further study the catalytic effect of TA-Pb/Cu shells. 2.4 % (mass fraction, equal to the mass fraction of TA-Pb/Cu shells of RDX@TA-Pb/Cu microcapsules) TA-Pb/Cu are added to RDX by physical mixing. The obtained RDX + TA-Pb/Cu physical mixtures are further characterized to study the catalytic effects of *in situ* self-assembly coating.

3. Results and discussions

3.1. Surface element analysis and crystal structure of RDX@TA-Pb/Cu microcapsules

XPS is used to characterize the surface element of RDX and RDX@TA-Pb/Cu microcapsules. Full XPS spectra can be used to judge whether TA-Pb/Cu shells have been introduced to the surface of RDX, in that the element types of TA-Pb/Cu shells are different with RDX. Full XPS spectra of RDX and RDX@TA-Pb/Cu microcapsules are listed in Fig. 2a. It can be concluded from Fig. 2a that all of the main peaks of pure RDX can be indexed to C1s, N1s, and O1s electrons exclusively, which originates from RDX crystal. For RDX@TA-Pb/Cu microcapsules, Pb4f and Cu2p peaks are detected in XPS survey spectra, demonstrating that TA-Pb/Cu shells are formed and coated on the surface of RDX. In addition, the high-resolution spectra of RDX and TA-Pb/Cu shells show distinct differences. Therefore, high-resolution spectra of XPS can be used to further confirmation of the surface structure of RDX@TA-Pb/Cu microcapsules. In this study, Avantage software is used to perform XPS analyses. A linear background representation is adopted for the C1s XPS spectrum (Major et al., 2020), and a mixed Gaussian-Lorentzian product function is used in XPS peak fitting (Jain et al., 2018; Townsend and Tou, 1980). The high-resolution XPS spectrum of C1s region of RDX, TA-Pb/Cu and RDX@TA-Pb/Cu microcapsules are shown in Fig. 2b. C1s region of RDX can be divided into two peaks, assigned to C—H (285.08 eV) and N—C—N (287.98 eV). C1s region of TA-Pb/Cu can be divided into three peaks, assigned to C—H, C—C (284.78 eV), C-OH (286.38 eV) and C═O (287.78 eV). The peak shapes of C1s of RDX@TA-Pb/Cu microcapsules have much differences with pure RDX. Compared with pure RDX, the intensity of the peak around 284 eV of RDX@TA-Pb/Cu microcapsules are significantly increased because many C—C and C—H (originating from TA) are introduced to the surface of RDX. In addition, compared with pure RDX, C-OH peak (originating from TA) is detected on RDX@TA-Pb/Cu microcapsules. For high-resolution spectrum, the variation of peak intensity and the emergence of new peak illustrate that the surface element has been changed after coating. Above all, the emergence of Pb4f and Cu2p peaks on full XPS spectra and the variation of C1s high-resolution spectrum illustrate that TA-Pb/Cu shells have been successfully introduced to the surface of RDX.

The crystal structures of RDX, TA-Pb/Cu, RDX@TA-Pb/Cu microcapsules and RDX + TA-Pb/Cu physical mixtures are characterized by XRD and FT-IR. XRD patterns of different samples are listed in Fig. 3a. Sharp and well-defined peaks are showed on the XRD pattern of RDX due to the crystalline structure of RDX. No obviously peaks are detected on TA-Pb/Cu XRD pattern, illustrating that TA-Pb/Cu are amorphous structure. After coating with TA-Pb/Cu shells, the characteristic peaks of RDX still exist, illustrating that the crystal form of RDX are not changed. The XRD pattern of RDX agree with RDX@TA-Pb/Cu microcapsules well, illustrating that *in situ* self-assembly coating has no influence on the crystal structure of RDX. XRD results reflected that the crystalline phase remained stable during the coating process. FT-IR spectra of different samples are illustrated in Fig. 3b. It can be concluded from Fig. 3b that the FT-IR spectra of RDX@TA-Pb/Cu microcapsules are consistent with RDX well, illustrating that the chemical structures of RDX remain stable during the coating process. The content of TA-Pb/Cu in RDX@TA-Pb/Cu microcapsules is low, resulting that the characteristic peaks of TA-Pb/Cu cannot be detected on FT-IR spectrum of RDX@TA-Pb/Cu microcapsules. Therefore, it can be deduced from XRD and FT-IR results that the physical and chemical

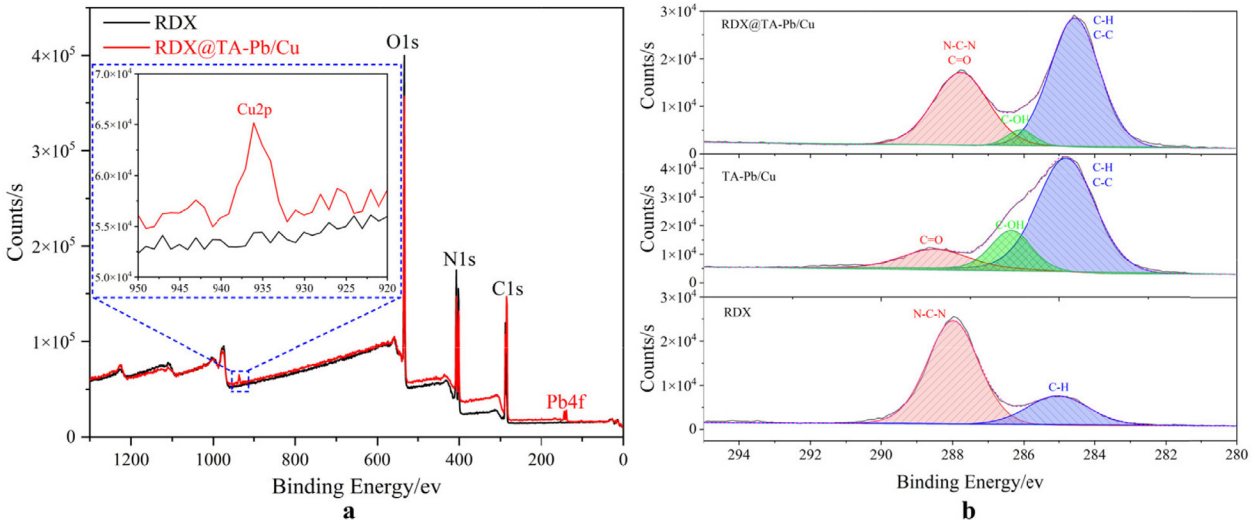

Fig. 2 A Full XPS spectra of RDX and RDX@TA-Pb/Cu microcapsules, b C1s XPS spectra of RDX, TA-Pb/Cu and RDX@TA-Pb/Cu microcapsules.

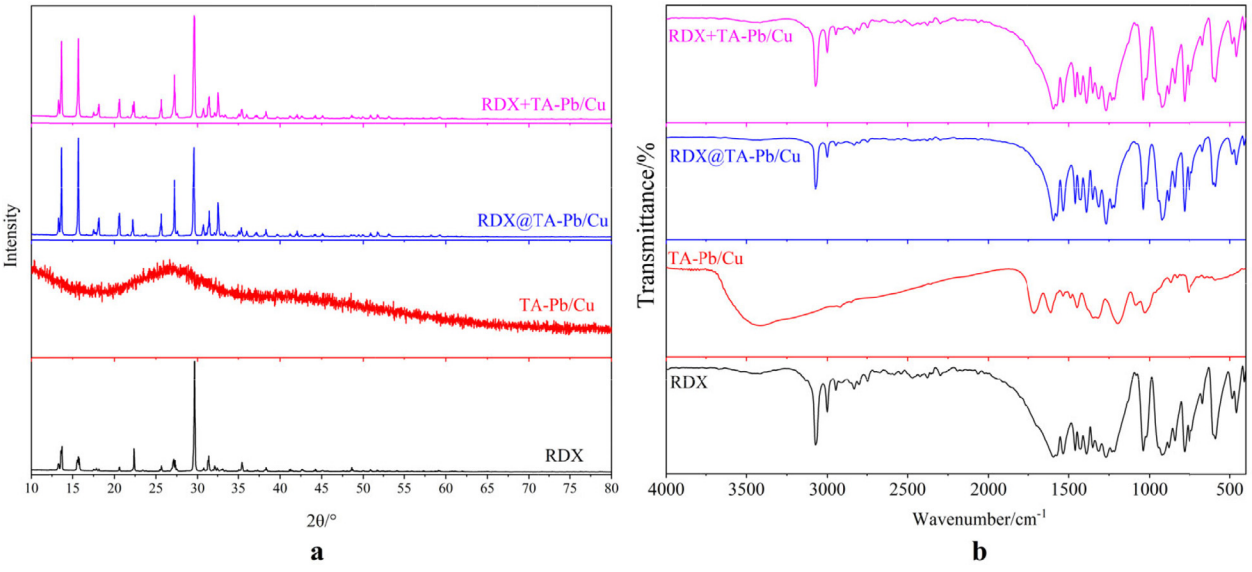

Fig. 3 XRD patterns (a) and FT-IR spectra (b) of RDX, TA-Pb/Cu, RDX@TA-Pb/Cu microcapsules and RDX + TA-Pb/Cu physical mixtures.

properties of RDX have not changed during *in situ* self-assembly coating process.

3.2. Surface topography of RDX@TA-Pb/Cu microcapsules

It can be concluded from XPS results that TA-Pb/Cu has been introduced to the surface of RDX, but XPS cannot provide the detailed microstructure surface topography of RDX@TA-Pb/Cu microcapsules. SEM is used to further characterize the coating effects of TA-Pb/Cu shells on RDX surfaces, and the characterization results are shown in Fig. 4. It can be concluded from Fig. 4a that the surface of RDX is smooth due to the crystallization process. Fig. 4b displays the microstructure surface topography of RDX@TA-Pb/Cu microcapsules, which obviously shows that TA-Pb/Cu shells are formed and uniformly coated on the surfaces of RDX. In addition, the thickness of TA-Pb/Cu shells coated on RDX surface is around 150 nm, which can protect RDX when suffering external stimulus, and thus ameliorating the mechanical and thermal sensitivity of RDX. The surface of TA-Pb/Cu shells are roughness, which can enlarge accessible surface area with adhesives when preparing RDX-CMDB propellants, and thus ameliorating the mechanical properties. During *in situ* reaction process, TA-Pb/Cu films are first formed in solutions, and then adsorbed on RDX surfaces due to the non-bond interaction between TA-Pb/Cu films and RDX surfaces. During SEM measurements, when the energy of electron beam is high, RDX surfaces are easily crack and become wrinkled, while the surface of RDX@TA-Pb/Cu microcapsules are much stabler under the same condition, indicating that RDX crystals become obviously resistant to electronic beam under protection of TA-Pb/Cu shells. The elemental composition of

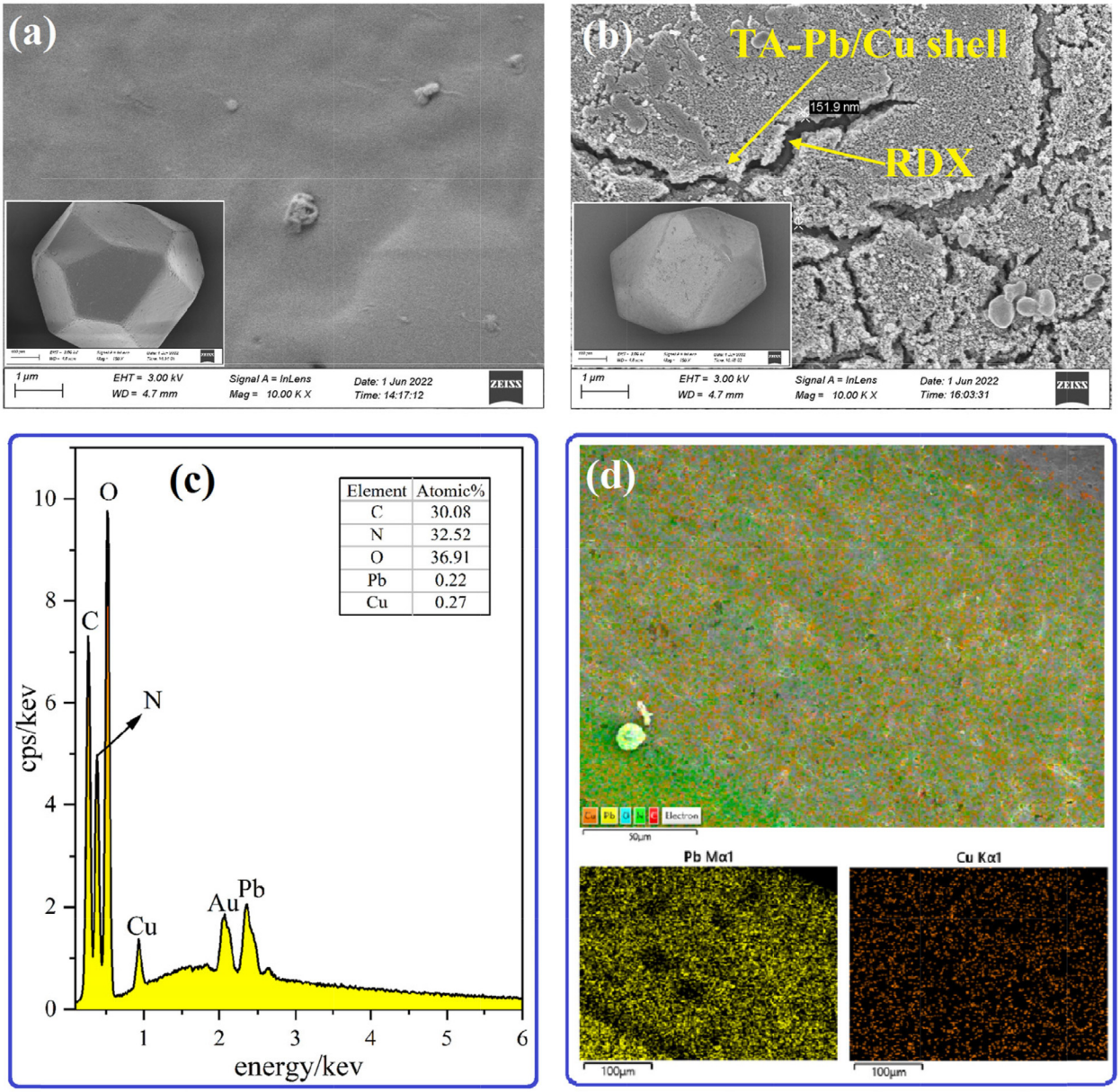

Fig. 4 A surface morphology of rdx, b surface morphology of rdx@ta-pb/cu microcapsules, c eds of rdx@ta-pb/cu microcapsules, d element mapping of c, n, o, pb and cu.

RDX@TA-Pb/Cu microcapsules is investigated by EDS spectrum as shown in Fig. 4c. Pb and Cu are present on EDS spectrum due to the *in situ* self-assembly coating. The number of Pb and Cu are almost the same, illustrating that *in situ* reaction conditions are suitable. The elemental mapping of C, N, O, Pb and Cu in RDX@TA-Pb/Cu microcapsules is shown in Fig. 4d. The results show that Pb and Cu are homogeneously coated on RDX surfaces, which may enhance the catalytic effect of TA-Pb/Cu.

3.3. Mechanical sensitivities and explosion points of RDX@TA-Pb/Cu microcapsules

XPS, SEM and EDS results demonstrate that TA-Pb/Cu shells have been successfully coated on RDX surfaces. The TA-Pb/Cu shells can protect the core RDX, and thus decrease the mechanical and thermal hazards of RDX. The impact sensitivity, friction sensitivity and explosion point (5 s delay method) of RDX, RDX + TA-Pb/Cu physical mixtures and RDX@TA-Pb/Cu microcapsules are measured according GJB 772A to evaluate the influences of TA-Pb/Cu shells on mechanical and thermal safeties of RDX. The mass fraction of TA-Pb/Cu is 2.4 %, which is the same with that of RDX@TA-Pb/Cu microcapsules. The obtained results are summarized in Table 1.

Mechanical sensitivities results show that both the impact sensitivity and friction sensitivity are decreased after coating with TA-Pb/Cu shells, illustrating that the mechanical hazards are decreased. *In situ* self-assembly coating technique can facilitate extraordinarily high coverage and shell strength owing to the chemical reaction occurred on the surface of RDX. High strength TA-Pb/Cu shells endow RDX hard armors that can

Table 1 Impact sensitivity, friction sensitivity and explosion point of RDX, RDX + TA-Pb/Cu physical mixtures and RDX@TA-Pb/Cu microcapsules.

parameters	RDX	RDX + TA-Pb/Cu	RDX@TA-Pb/Cu
impact sensitivity/%	84	76	48
friction sensitivity/%	72	76	40
explosion point/℃	257	254	268

protect RDX crystals when suffering external mechanical stimulations and thus decrease the mechanical sensitivities. The mechanical sensitivities of RDX + TA-Pb/Cu physical mixtures are close to that of RDX, illustrating that physical mixing has few influences on the mechanical safety of RDX. Compared with RDX, the explosion points of RDX@TA-Pb/Cu microcapsules increase from 257 °C to 268 °C, illustrating that the thermal sensitivities are decreased. TA-Pb/Cu is a heat-resistant material, whose decomposition temperature (331.83 °C, Fig. 5) are higher than that of RDX (244.49 °C, Fig. 5). Therefore, TA-Pb/Cu shells can decline the heat transportation rate and absorb some heat during the measurements, resulting in higher explosion points of RDX@TA-Pb/Cu microcapsules. The explosion points of RDX + TA-Pb/Cu physical mixtures are close to that of RDX, illustrating that physical mixing has few influences on the thermal safety of RDX. Above all, the mechanical and thermal safeties of RDX can be obviously enhanced by coating with TA-Pb/Cu shells.

3.4. Non-isothermal decomposition of RDX@TA-Pb/Cu microcapsules

DSC is used to characterize the non-isothermal decomposition properties of RDX@TA-Pb/Cu microcapsules at a heating rate of 10 °C·min^{-1} with nitrogen atmosphere. The obtained DSC results of RDX, TA-Pb/Cu, RDX@TA-Pb/Cu microcapsules and RDX + TA-Pb/Cu physical mixtures are summarized in Fig. 5. The mass fraction of TA-Pb/Cu is 2.4 %, which is the same with that of RDX@TA-Pb/Cu microcapsules.

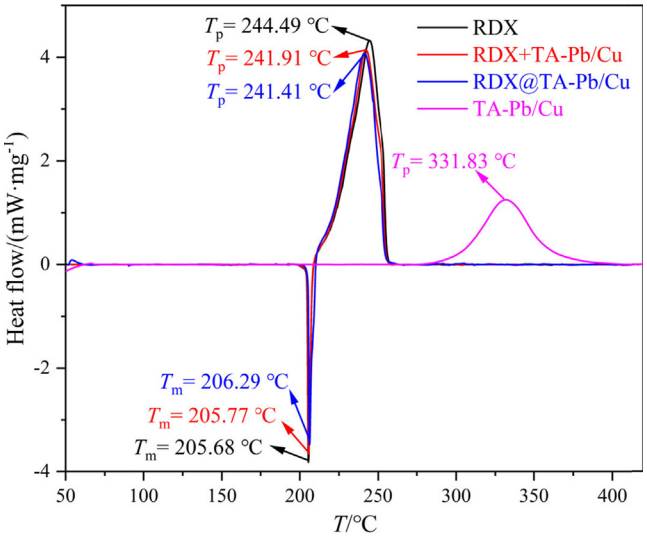

Fig. 5 DSC results of RDX, TA-Pb/Cu, RDX@TA-Pb/Cu microcapsules and RDX + TA-Pb/Cu physical mixtures.

DSC results demonstrate that the melting point (T_m) of RDX, RDX@TA-Pb/Cu microcapsules and RDX + TA-Pb/Cu physical mixtures are almost the same (around 206 °C), illustrating that the introduce of TA-Pb/Cu by *in situ* coating or physical mixing has few influences on the melting process of RDX. The decomposition temperature (T_p) of TA-Pb/Cu are higher than RDX, illustrating that TA-Pb/Cu can enhance the heat resistance of RDX, which can interpret why the explosion points of RDX@TA-Pb/Cu microcapsules are higher than that of RDX. Compared with

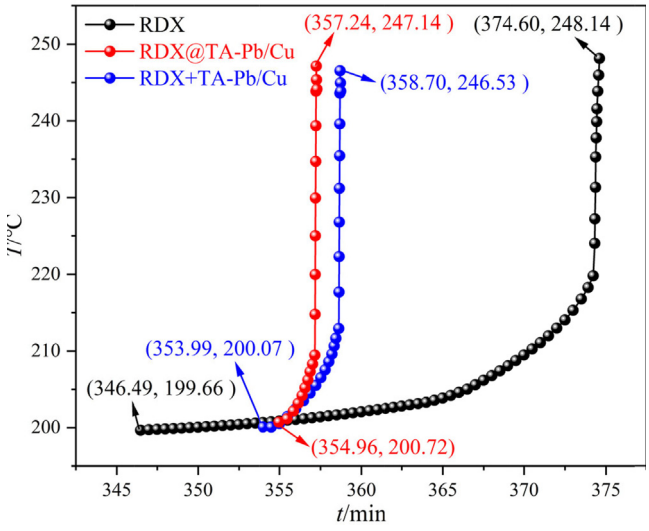

Fig. 6 ARC results of RDX, RDX@TA-Pb/Cu microcapsules and RDX + TA-Pb/Cu physical mixtures.

Table 2 Adiabatic thermal decomposition parameters of RDX, RDX@TA-Pb/Cu microcapsules and RDX + TA-Pb/Cu physical mixtures.

parameters	RDX	RDX@TA-Pb/Cu	RDX + TA-Pb/Cu
sample mass/g	0.1207	0.1204	0.1206
T_0/℃	199.66	200.72	200.07
t_0/min	346.49	354.96	353.99
T_f/℃	248.14	247.14	246.53
t_f/min	374.60	357.24	358.70
ΔT_{ad}/℃	48.48	46.42	46.46
β_m/(℃·min^{-1})	355.68	532.36	474.86
Δt/min	28.11	2.28	4.71

pure RDX, the T_p of RDX@TA-Pb/Cu microcapsules and RDX + TA-Pb/Cu physical mixtures decreased from 244.49 °C to 241.41 °C and 241.91 °C, respectively. In addition, the initial decomposition temperature (T_0) of RDX, RDX@TA-Pb/Cu microcapsules and RDX + TA-Pb/Cu physical mixtures are almost the same (around 211 °C), illustrating that the introduce of TA-Pb/Cu will not decrease the thermal stability of RDX. Therefore, the $T_p - T_0$ of RDX is longer than that of RDX@TA-Pb/Cu microcapsules and RDX + TA-Pb/Cu physical mixtures, illustrating that both physical mixing and *in situ* self-assembly coating of TA-Pb/Cu can catalyze the thermal decomposition process of RDX. However, it difficult to judge the catalytic effect of physical mixing and *in situ* self-assembly coating through DSC results. Moreover, the decomposition process of TA-Pb/Cu are not detected on DSC curves of RDX@TA-Pb/Cu microcapsules and RDX + TA-Pb/Cu physical mixtures, in that the content of TA-Pb/Cu is low. When RDX decomposed, a large amount of energy are released rapidly, which will accelerate the decomposition process of TA-Pb/Cu for both RDX@TA-Pb/Cu microcapsules and RDX + TA-Pb/Cu physical mixtures.

3.5. Catalytic effects of TA-Pb/Cu shells on RDX

DSC results show that both physical mixing and *in situ* self-assembly coating of TA-Pb/Cu can catalyze the thermal decomposition process of RDX. But the catalytic effect of physical mixing and *in situ* self-assembly coating cannot be expressed quantitatively. In this study, ARC is further used to study the catalytic effects of TA-Pb/Cu on thermal decomposition of RDX. During ARC measurements, the decomposition process is sample controlled and not forced from outside, which is an effective method to study the catalytic effects of TA-Pb/Cu shells on RDX. 120 ± 1 mg RDX, RDX@TA-Pb/Cu microcapsules and RDX + TA-Pb/Cu physical mixtures are measured using heat-wait-search (HWS) procedure with temperature increment of 5 °C, repectively (Townsend and Tou, 1980; Zhang et al., 2016). The obtained exothermic processes of different samples are summarized in Fig. 6. The obtained initial decomposition temperature (T_0), initial decomposition time (t_0), final decomposition temperature (T_f), final decomposition time (t_f), adiabatic temperature rise (ΔT_{ad}), maximum temperature rise rate (β_m) and whole decomposition period (Δt) are listed in Table 2.

ARC measured results show that the T_0 of RDX, RDX@TA-Pb/Cu microcapsules and RDX + TA-Pb/Cu physical mixtures are almost the same (around 200 °C), illustrating that the introduce of TA-Pb/Cu by *in situ* coating or physical mixing has few influences on the adiabatic stability of RDX. The ΔT_{ad} of RDX@TA-Pb/Cu microcapsules and RDX + TA-Pb/Cu physical mixtures are lower than RDX, due to the introduction of TA-Pb/Cu with low energy density. Compared with pure RDX, the β_m of RDX@TA-Pb/Cu microcapsules and RDX + TA-Pb/Cu physical mixtures increase from 355.68 °C·min^{-1} to 532.36 °C·min^{-1}, and 477.86 °C·min^{-1}, and the Δt decrease from 28.11 min to 2.28 min and 4.71·min, respectively. These phenomena illustrate that the decomposition rates of RDX are enhanced and the total decomposition period of RDX are decreased by A-Pb/Cu. The β_m of RDX@TA-Pb/Cu microcapsules are higher than that of RDX + TA-Pb/Cu physical mixtures, and the Δt of RDX@TA-Pb/Cu microcapsules are shorter than that of RDX + TA-Pb/Cu physical mixtures, illustrating that the catalytic effects of TA-Pb/Cu are better through *in situ* self-assembly coating.

Table 3 The E_a, A and $f(\alpha)$ of RDX, RDX@TA-Pb/Cu microcapsules and RDX + TA-Pb/Cu physical mixtures of adiabatic decomposition process.

No.	$f(\alpha)$	RDX			RDX@TA-Pb/Cu			RDX + TA-Pb/Cu		
		R^2	E_a/kJ·mol^{-1}	A/s^{-1}	R^2	E_a/kJ·mol^{-1}	A/s^{-1}	R^2	E_a/kJ·mol^{-1}	A/s^{-1}
1	$1/(2\alpha)$	0.6578	211.627	7.090×10^{17}	0.7459	156.503	1.847×10^{12}	0.7678	163.139	4.083×10^{13}
2	$2\alpha^{0.5}$	0.6578	−105.814	3.638×10^{-16}	0.7459	−78.251	3.924×10^{-13}	0.7678	−81.570	9.205×10^{-13}
3	$1-\alpha$	0.8847	93.505	1.093×10^{6}	0.8798	103.590	1.788×10^{7}	0.8851	101.442	5.125×10^{7}
4	$(1-\alpha)^2$	**0.9547**	**298.315**	**2.696×10^{26}**	0.8798	207.180	3.857×10^{18}	0.8851	202.883	6.397×10^{18}
5	$2(1-\alpha)^{3/2}$	0.8847	140.258	7.556×10^{10}	0.8798	155.385	4.152×10^{12}	0.8851	152.162	9.053×10^{12}
6	$[-\ln(1-\alpha)]^{-1}$	0.7445	250.671	7.011×10^{21}	0.8480	199.466	4.707×10^{16}	0.8591	205.449	8.785×10^{17}
7	$3/2(1-\alpha)^{2/3}[1-(1-\alpha)^{1/3}]^{-1}$	0.9199	287.010	2.088×10^{26}	**0.9634**	**252.280**	**6.269×10^{21}**	**0.9679**	**257.138**	**8.790×10^{22}**
8	$3/2(1+\alpha)^{2/3}[(1+\alpha)^{1/3}-1]^{-1}$	0.5868	180.562	2.881×10^{13}	0.6566	124.852	6.445×10^{7}	0.6861	131.247	1.359×10^{9}
9	$3/2(1-\alpha)^{2/3}[-ln(1-\alpha)]^{1/3}$	0.0042	9.948	1.468×10^{-3}	0.2756	37.101	1.439	0.2322	32.959	2.651
10	$4(1-\alpha)[-\ln(1-\alpha)]^{4/3}$	0.3443	−94.498	7.426×10^{-15}	0.1858	−46.010	1.215×10^{-9}	0.2443	−52.645	1.288×10^{-9}
11	$3\alpha^{2/3}$	0.6578	−141.085	5.660×10^{-20}	0.7459	−104.335	5.535×10^{-16}	0.7678	−108.760	1.012×10^{-15}
12	$3(1-\alpha)^{2/3}$	0.8847	62.337	1.364×10^{2}	0.8798	69.060	9.936×10^{2}	0.8851	67.628	3.418×10^{3}
13	$2(1-\alpha)^{1/2}$	0.8847	46.753	3.956	0.8798	51.795	1.924×10	0.8851	50.721	7.253×10
14	$3(1-\alpha)[-\ln(1-\alpha)]^{2/3}$	0.2766	−73.609	1.478×10^{-12}	0.0748	−29.388	8.689×10^{-8}	0.1234	−35.524	1.029×10^{-7}
15	$2(1-\alpha)[1-\ln(1-\alpha)]^{1/2}$	0.8386	67.505	7.440×10^{2}	0.8355	75.704	7.687×10^{3}	0.8411	73.762	2.335×10^{4}
16	$2/3[(1-\alpha)^{-1/3}-1]^{-1}$	0.7745	267.146	2.269×10^{23}	0.8771	217.750	2.352×10^{18}	0.8850	223.325	3.957×10^{19}

To further study the catalytic effect of TA-Pb/Cu, the activation energies (E_a), pre-exponential factors (A) and mechanism functions ($f(\alpha)$) of adiabatic decomposition process of RDX, RDX@TA-Pb/Cu microcapsules and RDX + TA-Pb/Cu physical mixtures are calculated using the mechanism functions method (Jain et al., 2018; Townsend and Tou, 1980). The 16 kinetic models and calculation results are depicted in Table 3.

The calculation results show that the adiabatic decomposition mechanism function of RDX is $(1-\alpha)^2$, while the adiabatic decomposition mechanism functions of RDX@TA-Pb/Cu microcapsules and RDX + TA-Pb/Cu physical mixtures all are $3/2(1-\alpha)^{2/3}[1-(1-\alpha)^{1/3}]^{-1}$, illustrating that the adiabatic decomposition process are change after the addition of TA-Pb/Cu. Compared with RDX, the E_a of RDX@TA-Pb/Cu microcapsules and RDX + TA-Pb/Cu physical mixtures decreased from 298.315 kJ·mol^{-1} to 252.280 kJ·mol^{-1} and 257.138 kJ·mol^{-1}, respectively, illustrating that TA-Pb/Cu can catalyze the adiabatic decomposition of RDX. Above all, both physical mixing and *in situ* self-assembly coating can catalyze the thermal decomposition process of RDX, while the catalytic effects of *in situ* self-assembly coating are better.

To further study the catalytic effect of TA-Pb/Cu shells on the combustion of RDX in air atmosphere, RDX, RDX@TA-Pb/Cu microcapsules and RDX + TA-Pb/Cu physical mixtures are combusted in the air atmosphere, and then the solid residues are collected for further analyses. The SEM image of the residues of RDX, RDX@TA-Pb/Cu microcapsules and RDX + TA-Pb/Cu physical mixtures are shown in Fig. 7. Fig. 7a illustrates that there are some blocky unreacted RDX left in RDX combustion residues due to the incomplete combustion. Fig. 7b is the combustion residues of RDX@TA-Pb/Cu microcapsules, which clearly shows that a PbCuO composite oxides shells are formed after RDX@TA-Pb/Cu microcapsules combustion. In addition, there are very few RDX left in PbCuO composite oxides shells, illustrating that the combustion of RDX@TA-Pb/Cu microcapsules is complete, and thus the catalytic effects of TA-Pb/Cu shells on RDX combustion is good. Fig. 7c demonstrates that many PbCuO composite oxides particles are generated after RDX + TA-Pb/Cu physical mixtures combustion. There are few blocky unreacted RDX left in combustion residues, illustrating that the addition of TA-Pb/Cu through physical mixing can catalyze the combustion of RDX as well. Fig. 7d is the elemental mapping of

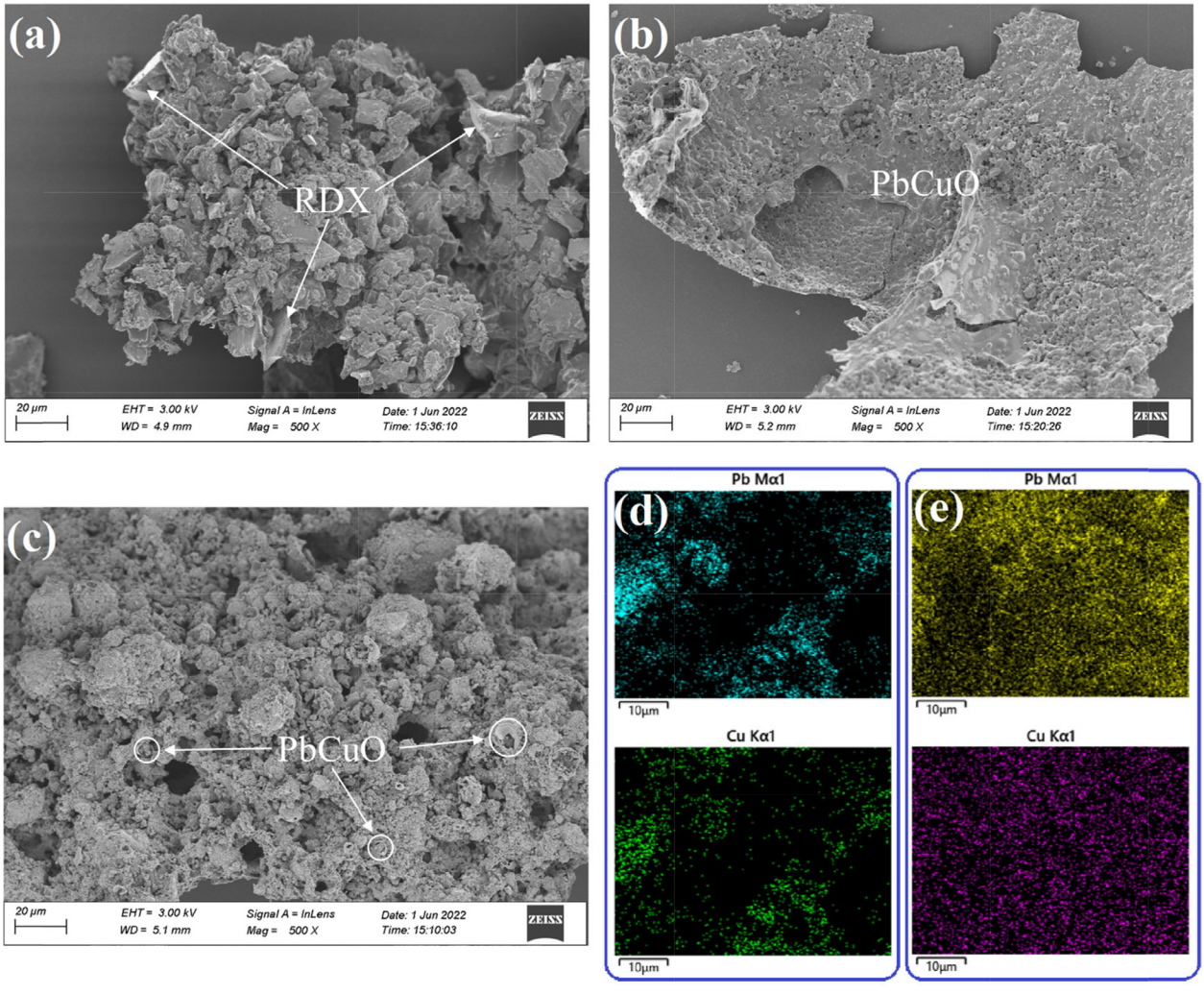

Fig. 7 A residue of rdx, b residue of rdx@ta-pb/cu microcapsules, c residue of rdx@ta-pb/cu physical mixtures, d element mapping of pb and cu of rdx@ta-pb/cu physical mixtures, e element mapping of pb and cu of rdx@ta-pb/cu microcapsules.

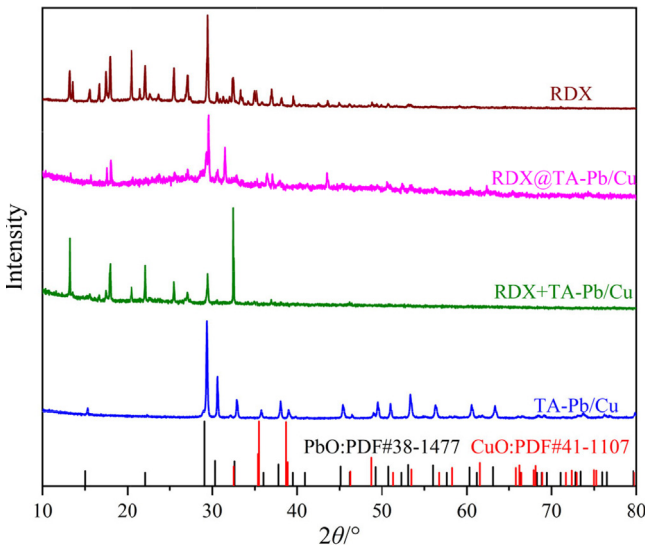

Fig. 8 XRD patterns of the residues of RDX, TA-Pb/Cu, RDX@TA-Pb/Cu microcapsules and RDX + TA-Pb/Cu physical mixtures.

Pb and Cu in combustion residues of RDX + TA-Pb/Cu physical mixtures, which shows that Pb and Cu elements are distributed mainly in some specific areas. The distribution of Pb and Cu elements (Fig. 7e) are homogeneous, resulting in more effective catalysis during the combustion process.

It is difficult to confirm whether RDX left in the combustion residues just by SEM. Therefore, XRD is further used to characterize the combustion residues. Fig. 8 displays the XRD patterns of the solid combustion residues of RDX, TA-Pb/Cu, RDX@TA-Pb/Cu microcapsules and RDX + TA-Pb/Cu physical mixtures. All characteristic peaks of RDX still exist on the RDX combustion residues, illustrating that there are some unreacted RDX left after RDX combustion in air atmosphere. For the combustion residues of RDX@TA-Pb/Cu microcapsules, there are very few characteristic peaks of RDX, illustrating that the combustion of RDX can be conducted thoroughly, and thus the catalytic effect of TA-Pb/Cu shells is good. The XRD patterns of the combustion residues of RDX@TA-Pb/Cu microcapsules are different with CuO and PbO, illustrating that the combustion residues of TA-Pb/Cu shells are composite oxides. In addition, the XRD patterns of the combustion residues of RDX@TA-Pb/Cu microcapsules are different with TA-Pb/Cu combustion residues as well, in that the combustion temperature of RDX@TA-Pb/Cu microcapsules is much higher than TA-Pb/Cu, which results in different structures. For the combustion residues of RDX + TA-Pb/Cu physical mixtures, there are some characteristic peaks of RDX with low intensity, illustrating that some RDX left after RDX + TA-Pb/Cu physical mixtures combustion in air atmosphere, which further demonstrates that the catalytic effect of TA-Pb/Cu can not be sufficiently exploited by physical mixing.

4. Conclusions

RDX@TA-Pb/Cu microcapsules are prepared via *in situ* self-assembly coating. XPS, SEM and EDS results show that TA-Pb/Cu shells are homogeneously coated on the surface of RDX. XRD and FT-IR results show that the chemical structures of RDX are not changed during the *in situ* self-assembly coating process. The mechanical and thermal sensitivities of RDX@TA-Pb/Cu microcapsules are remarkedly decreased, illustrating that the safety of RDX can be enhanced by coating with TA-Pb/Cu shells. The initial decomposition temperature of RDX@TA-Pb/Cu are almost the same with RDX, illustrating that TA-Pb/Cu shells have few influences on thermal stability of RDX. The decomposition periods of RDX@TA-Pb/Cu microcapsules and RDX + TA-Pb/Cu physical mixtures are lower than RDX, and the maximum temperature rise rate of RDX@TA-Pb/Cu microcapsules and RDX + TA-Pb/Cu physical mixtures are higher than RDX, illustrating that TA-Pb/Cu can catalyze the decomposition of RDX. Compared with RDX + TA-Pb/Cu physical mixtures, the decomposition periods of RDX@TA-Pb/Cu microcapsules are shorter and the combustion are more complete, illustrating that the introduction of TA-Pb/Cu by *in situ* self-assembly coating are better than physical mixing. Above all, TA-Pb/Cu shells can decrease the mechanical and thermal sensitivity of RDX and catalyze the thermal decomposition and combustion of RDX. In addition, the catalytic effect of *in situ* self-assembly coating is better than physical mixing.

Declaration of Competing Interest

The authors declare that they have no known competing financial interests or personal relationships that could have appeared to influence the work reported in this paper.

Acknowledgments

This work was supported by Fundamental Research Program of Shanxi Province (Grant No. 202103021223192).

References

Adhikari, S., Selvaraj, S., Kim, D.H., 2018. Adv. Mater. Interfaces 5, 1800581.
Damse, R.S., Singh, A., Singh, H., 2007. High energy propellants for advanced gun ammunition based on RDX, GAP and TAGN compositions. Propell. Explos. Pyrot. 32, 52–56.
Dubey, R., Srivastava, P., Kapoor, I.P.S., Singh, G., 2012. Synthesis, characterization and catalytic behavior of Cu nanoparticles on the thermal decomposition of AP, HMX, NTO and composite solid propellants. Thermochim. Acta 549, 102–109.
Ejima, H., Richardson, J.J., Liang, K., Best, J.P., van Koeverden, M. P., Such, G.K., Cui, J., Caruso, F., 2013. One-step assembly of coordination complexes for versatile film and particle engineering. Science 341, 154–157.
Elbasuney, S., Fahd, A., Mostafa, H.E., 2017. Combustion characteristics of extruded double base propellant based on ammonium perchlorate/aluminum binary mixture. Fuel 208, 296–304.
Gong, H., Xiao, Z., Zhuang, Y., Liang, S., Li, X., Zheng, W., Duan, A., Zhang, X., Liu, J., 2021. Core-shell meso-beta@mesoporous aluminosilicate supported Ni2P catalyst for the hydrodenitrogenation of quinoline: effect of core shell structure on Ni_2P particle size. Fuel 302, 121131.
Gong, Y., Yuan, Y., Chen, C., Chaemchuen, S., Verpoort, F., 2020. Palladium metallated shell layer of shell@core MOFs as an example of an efficient catalyst design strategy for effective olefin hydrogenation reaction. J. Catal. 392, 141–149.
Gong, F.Y., Zhang, J.H., Ding, L., Yang, Z.J., Liu, X.B., 2017. Mussel-inspired coating of energetic crystals: a compact core-shell structure with highly enhanced thermal stability. Chem. Eng. J. 309, 140–150.
Guo, J., Ping, Y., Ejima, H., Alt, K., Meissner, M., Richardson, J.J., Yan, Y., Peter, K., vonElverfeldt, D., Hagemeyer, C.E., Caruso, F., 2014. Engineering multifunctional capsules through the assem-

bly of metal-phenolic networks. Angew. Chem. Int. Ed. Engl. 53, 5546–5551.
He, S., Lehmann, S., Bahrami, A., Nielsch, K., 2021. Current state-of-the-art in the interface/surface modification of thermoelectric materials. Adv. Energy Mater., 2101877
He, S., Bahrami, A., Zhang, X., Martínez, I.G., Lehmann, S., Nielsch, K., 2022. Effect of powder ALD interface modification on the thermoelectric performance of bismuth. Adv. Mater. Technol. 7, 2100953.
He, W., Liu, P., Gong, F., Tao, B., Gu, J., Yang, Z., Yan, Q., 2018. Tuning the reactivity of metastable intermixed composite n–Al/PTFE by polydopamine interfacial control. ACS Appl. Mater. Interfaces 10, 32849–32858.
Jain, V., Biesinger, M.C., Linford, M.R., 2018. The Gaussian-Lorentzian sum, product, and convolution (voigt) functions in the context of peak fitting X-ray photoelectron spectroscopy (XPS) narrow scans. Appl. Surf. Sci. 447, 548.
Jiang, Q., Luo, Y., Yang, F., Ju, R., Zhang, M., Wang, W., Li, B., 2020. Influence of lead and copper salt catalysts on the thermal decomposition and cook-off responses of DNTF. Chin. J. Energ. Mater. 28, 470–474.
Lan, G., Jin, S., Chen, M., Li, J., Lu, Z., Wang, N., Li, L., 2020. Preparation and performances characterization of HNIW/NTO-based high-energetic low vulnerable polymer-bonded explosive. J. Therm. Anal. Calorim. 139, 3589–3602.
Lan, G., Jin, S., Chen, M., Li, J., Du, L., Wang, J., Chen, K., Li, L., 2020. Preparation and thermal properties study of HNIW/FOX-7 based high energy polymer bonded explosive (PBX) with low vulnerability to thermal stimulations. J. Energ. Mater. 38, 83–97.
Lan, G., Zhang, G., Chao, H., Li, Z., Wang, J., Li, J., 2022. Ameliorating the performances of 3,4-bis(4′ -nitrofurazano-3′ -yl)furoxan (DNTF) by establishing tannic acid (TA) interface layer on DNTF surface. Chem. Eng. J. 434, 134513.
Lan, G., Zhang, G., Shen, J., Li, Z., Wang, J., Li, J., 2022. Establishing the interface layer on the pentaerythritol tetranitrate surface *via in situ* reaction. Langmuir 38, 12016–12023.
Le, T.T., Shilpa, K., Lee, C., Han, S., Weiland, C., Bare, S.R., Dauenhauer, P.J., Rimer, J.D., 2022. Core-shell and egg-shell zeolite catalysts for enhanced hydrocarbon processing. J. Catal. 405, 664–675.
Li, Z., Zhao, X., Gong, F., Lin, C., Liu, Y., Yang, Z., Nie, F., 2020. Multilayer deposition of metal-phenolic networks for coating of energetic crystals: modulated surface structures and highly enhanced thermal stability. ACS Appl. Energy Mater. 3, 11091–11098.
Liu, S., Du, B., Zhang, J., Pan, B., Li, W., Xie, G., 2001. Applied studies of new energetic catalysts in the screw extruded energetic propellant with low signature. Chin. J. Energ. Mater. 9, 130–131.
Liu, J., Ke, X., Xiao, L., Hao, G., Rong, Y., Jin, C., Jiang, W., Li, F., 2018. Application and properties of nano-sized RDX in CMDB propellant with low solid content. Propell. Explos. Pyrot. 43, 144–150.
Major, G.H., Farley, N., Sherwood, P.M.A., Linford, M.R., Terry, J., Fernandez, V., Artyushkova, K., 2020. Practical guide for curve fitting in X-ray photoelectron spectroscopy. J. Vac. Sci. Technol. A 38, 061203.
Näslund, L.Å., Persson, I., 2022. XPS spectra curve fittings of $Ti_3C_2T_x$ based on first principles thinking. Appl. Surf. Sci. 593, 153442.
Ou, Y.X., 2014. Explosives. Beijing Institute of Technology Press, Beijing.
Sánchez-Martín, J., Beltrán-Heredia, J., Gibello-Pérez, P., 2011. Adsorbent biopolymers from tannin extracts for water treatment. Chem. Eng. J. 168, 1241–1247.
Şengil, İ.A., Özacar, M., 2008. Biosorption of Cu (II) from aqueous solutions by mimosa tannin gel. J. Hazard. Mater. 157, 277–285.
Stepanov, V., Willey, T.M., Ilavsky, J., Gelb, J., Qiu, H., 2013. Structural characterization of RDX-based explosive nanocomposites. Propell. Explos. Pyrot. 38, 386–393.
Townsend, D.I., Tou, J.C., 1980. Thermal hazard evaluation by an accelerating rate calorimeter. Thermochim. Acta 37, 1–30.
Wei, J., Wang, G., Chen, F., Bai, M., Liang, Y., Wang, H., Zhao, D., Zhao, Y., 2018. Sol-gel synthesis of metal-phenolic coordination spheres and their derived carbon composites. Angew. Chem. Int. Ed. Engl. 57, 9838–9843.
Xiao, F., Liang, T., 2021. Preparation of hierarchical core-shell Al-PTFE@TA and Al-PTFE@TA-Fe architecture for improving the combustion and ignition properties of aluminum. Surf. Coat. Tech. 412, 127073.
Xiao, F., Liu, Z., Liang, T., Yang, R., Li, J., Luo, P., 2021. Establishing the interface layer on the aluminum surface through the self-assembly of tannic acid (TA): Improving the ignition and combustion properties of aluminum. Chem. Eng. J. 420, 130523.
Xu, G., Zhu, X., 2022. A core-shell structured Zn/ZSM-5@MCM-41 catalyst: preparation and enhanced catalytic properties in propane aromatization. Fuel 317, 123456.
Yang, Z., Ding, L., Wu, P., Liu, Y., Nie, F., Huang, F., 2015. Fabrication of RDX, HMX and CL-20 based composites via in situ polymerization of melamineformaldehyde resins with reduced sensitivity. Chem. Eng. J. 268, 60–66.
Yang, S.L., Meng, K.J., Xie, W., Nie, H., Yan, Q.L., 2022. Thermal reactivity of metastable metal-based fuel Al/Co/AP: mutual interaction mechanisms of the components. Fuel 315, 123203.
Yurtsever, M., Şengil, İ.A., 2009. Biosorption of Pb (II) ions by modified quebracho tannin resin. J. Hazard. Mater. 163, 58–64.
Zhang, G.Y., Jin, S.H., Li, L.J., Li, Z.H., Shu, Q.H., Wang, D.Q., Zhang, B., Li, Y.K., 2016. Evaluation of thermal hazards and thermo-kinetic parameters of 3-amino-4-amidoximinofurazan by ARC and TG. J. Therm. Anal. Calorim. 126, 1223–1230.
Zhang, S., Kou, K., Zhang, J., Jia, Q., Xu, Y., 2019. Compact energetic crystals@urea-formaldehyde resin micro-composites with evident insensitivity. Compos. Commun. 15, 103–107.
Zhang, D., Quayle, M.J., Petersson, G., Van Ommen, J.R., Folestad, S., 2017. Atomic scale surface engineering of micro- to nano-sized pharmaceutical particles for drug delivery applications. Nanoscale 9, 11410–11417.
Zhang, M., Zhao, F., Li, H., Yuan, Z., Dong, S., Wang, Y., Chen, X., Yang, Y., Song, X., Jiang, Z., 2022. Insight into graphene-salen metal nanocomposites on combustion performance and mechanism of HMX-CMDB propellant. Chem. Eng. J. 429, 132175.
Zhao, C.Y., Zhang, G.H., 2011. Review on microencapsulated phase change materials (MEPCMs): fabrication, characterization and applications. Renew. Sust. Energ. Rev. 15, 3813–3832.
Zou, Z., Chen, C., Hu, Z., Shen, Y., Fu, Z., Li, W., Zhang, Y., Zhang, H., Zhao, H., Wang, G., 2022. Core shell hetero-structured SiO2@Ni/SiO2 catalyst for efficient aqueous-phase hydrogenation of bio-derived unsaturated compounds. Fuel 318, 123694.